

Article

Model Development and Hindcast Simulations of NOAA's Integrated Northern Gulf of Mexico Operational Forecast System

Zizang Yang ^{1,*}, Lianyuan Zheng ², Phillip Richardson ¹, Edward Myers ¹ and Aijun Zhang ²

¹ NOAA/National Ocean Service/Coast Survey Development Laboratory, 1315 East-West Highway, Silver Spring, MD 20910, USA; phil.richardson@noaa.gov (P.R.); edward.myers@noaa.gov (E.M.)

² NOAA/National Ocean Service/Center for Operational Oceanographic Products and Services, 1305 East-West Highway, Silver Spring, MD 20910, USA; lianyuan.zheng@noaa.gov (L.Z.); aijun.zhang@noaa.gov (A.Z.)

* Correspondence: zizang.yang@noaa.gov; Tel.: +1-240-847-8255

Received: 2 October 2018; Accepted: 6 November 2018; Published: 12 November 2018



Abstract: NOAA's National Ocean Service is upgrading three existing northern Gulf of Mexico (GOM) operational nowcast/forecast systems (OFS) by integrating them into one single system (INGOFS) and developing additional domain coverage to encompass the lower Mississippi River, Lake Pontchartrain, Texas coastal embayments, and Mexican coastal waters. The system will produce real-time nowcast and short-range forecast guidance for water levels, 3-dimensional currents, water temperature, and salinity. INGOFS will be implemented using the Finite Volume Community Ocean Model (FVCOM). This paper describes the model configuration and results from a one-year (2 August 2016–1 August 2017) hindcast simulation. The model grid is composed of about 300,000 nodes and 600,000 elements, and has a spatial resolution ranging from 45 m near the coast to around 10 km on the open ocean boundary. It uses the FVCOM wetting and drying feature, the quadratic bottom friction scheme, and the two-equation model of the Mellor-Yamada Level 2.5 turbulence closure scheme. The hindcast results of water levels, surface temperatures, and salinity were verified by comparing the model time series with in situ observations. The root-mean-squared errors are about 0.08 m for water levels, about 1.1 °C for temperatures, and about 3.7 psu for salinity. The hindcast configuration will be further tested in a nowcast/forecast environment for a one-year period. The upgraded system is anticipated to be in operational production in mid-2020.

Keywords: Gulf of Mexico; operational nowcast and forecast system; Finite Volume Community Ocean Model; water level; temperature; salinity

1. Introduction

Coastal waters of the northern Gulf of Mexico (NGOM) encompass broad coastal regions spanning from the coast of Mexico in the west to the U.S. Gulf Coast in the northwest, north, and northeast (Figure 1). The hydrodynamic states in the region are governed by fresh water inflows from river discharge, off shelf dynamics, wind forcing and heat flux across the air-sea interface, and tidal fields [1–6]. The coastal circulation field is characterized by the combined seasonal buoyancy-driven coastal currents and by intrusions onto the shelf of the Loop Currents. Cross-shelf exchanges via mixing are driven by episodic wind events and by intrusions onto the shelf of the Loop Currents. River runoff onto the shelf is highly variable. Both the Atchafalaya River and the Mississippi River flow onto the Louisiana shelf, with a combined annual average discharge of over 14,000 m³/s [7]. The major portion of this runoff flows westward onto the west Louisiana shelf and the remaining portion flow

Tides in the NGOM region are modest [4], with either diurnal or mixed characteristics. The mean tidal amplitude ranges from several centimeters to less than 0.5 m. The strongest tidal currents are usually less than 15 cm/s. Using both mathematical analysis and one-dimensional water column numerical simulation, Burchard and Hetland [16] quantified the impact of tidal straining on the estuarine circulations. They found that without wind forcing and river inflows, tidal straining is responsible for about two-thirds of the estuarine circulation, while gravitational circulation is responsible for the remaining one-third.

The Gulf Coast is an area of active economic and recreational activities. The hydrographic and hydrodynamic states demonstrate significant impacts on the local ecosystem and daily human life. Operational hydrodynamic forecasting is of vital importance in support of harmful algal bloom (HAB) forecasts, marine navigation, emergency response, and the environmental management communities.

The National Oceanic and Atmospheric Administration (NOAA) currently has three operational oceanographic nowcast/forecast systems (OFS) for the NGOM region. These three OFS are the Northern Gulf of Mexico OFS (NGOFS), the nested northwest Gulf of Mexico OFS (NWGOFS), and the nested northeast OFS (NEGOFS) (<https://tidesandcurrents.noaa.gov/ofs/ngofs/ngofs.html>). The systems all use the Finite Volume Community Ocean Model (FVCOM) [17] as the core hydrodynamic model. They each produce eight-hour nowcasts and up to 48-hour forecast guidance of water levels, three-dimensional (3-D) currents, temperatures, and salinity fields. The three systems differ in their domain coverage, model grid resolution, and in their methods of applying open ocean boundary forcing [18,19].

Figure 2a depicts the domain of each system. Table 1 lists the size and spatial resolution of each model grid. The NGOFS domain spans the northern Gulf of Mexico coastal shelf from South Padre Island, Texas in the west to west of Panama City, Florida in the east. It lacks coverage of many alongshore estuaries and embayments and does not resolve fine coastline features. NWGOFS and NEGOFS were developed to partially resolve the NGOFS' limitations. Both NWGOFS and NEGOFS have higher spatial resolutions than NGOFS. NWGOFS covers Lake Charles, Sabine-Neches, Galveston, and Matagorda Bay, whereas NEGOFS covers Mobile Bay, Pascagoula, and the Gulfport area.

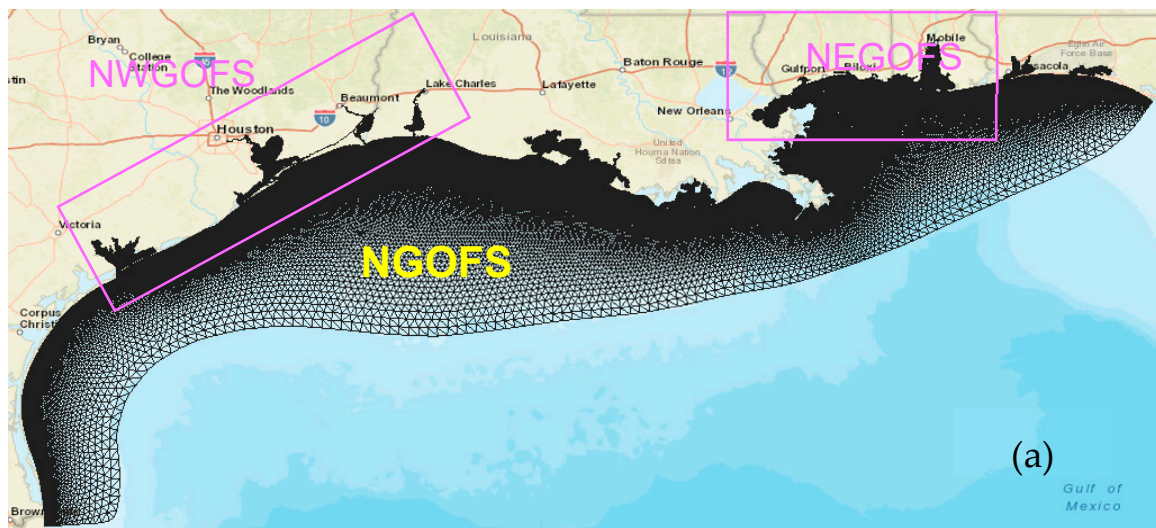


Figure 2. Cont.

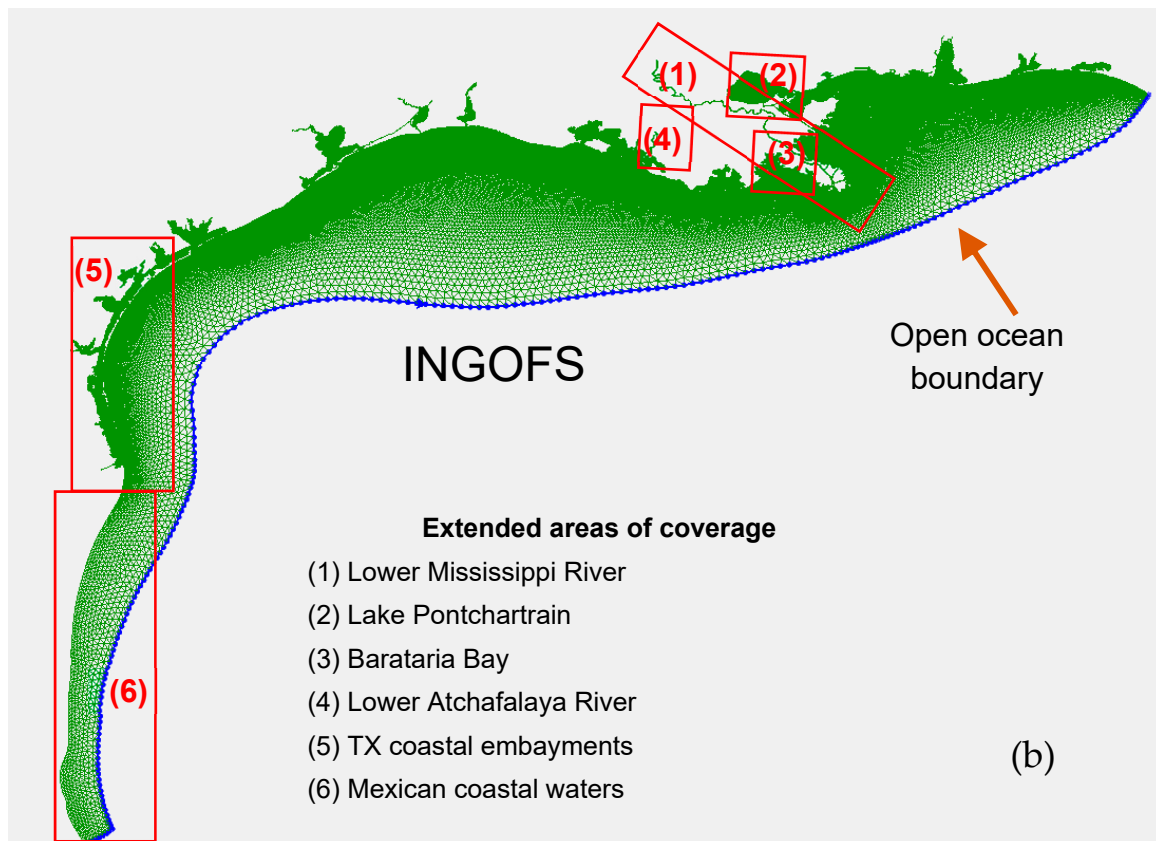


Figure 2. Model grids. (a) Combined grids of three existing OFS, and (b) the INGOFS grid.

Table 1. Dimension and resolution of NGOFS, NWGOFS, NEGOFs, and INGOFS model grids.

Model	Number of Nodes	Number of Elements	Element Size (min, max)
NGOFS	90,267	174,474	(150 m–11 km)
NWGOFS	85,707	160,444	(60 m–3.5 km)
NEGOFS	68,455	131,008	(45 m–2.2 km)
INGOFS	303,714	569,405	(45 m–11 km)

Figure 3 shows the diagram to illustrate the conceptual structure, forcing data inputs, system operations, analysis, and the archive of model outputs. The Center for Operational Oceanographic Products and Services (CO-OPS) implemented the OFS on the Weather and Climate Operational Supercomputing System (WCOSS), which is operated by the National Centers for Environmental Prediction (NCEP), Central Operations (NCO), of NOAA. The system runs make use of NCEP’s North American Mesoscale (NAM) outputs for the atmospheric forcing, and the U.S. Geological Survey (USGS) river discharge for the river forcing. The water levels, currents, water salinity, and water temperatures used by NGOFS for open boundary conditions (OBC) are generated from NCEP’s Global Real-Time Ocean Forecast System (G-RTOFS). The NEGOFs/NWGOFS OBC are taken from the NGOFS outputs via a one-way nesting approach [19]. The native formats of the forcing files are different from those required by FVCOM. The OFS (NGOFS, NEGOFs, and NWGOFS) use the Coastal Ocean Modeling Framework (COMF) [20] software package to transform the data sets into Network Common Data Form (NetCDF) files with data structures that conform to FVCOM requirements. Using the Continuous Operational Real-Time Monitoring System (CORMS) (<https://tidesandcurrents.noaa.gov/corms.html>), CO-OPS and NCO team up to monitor and log the system operations on a 24 × 7 basis.

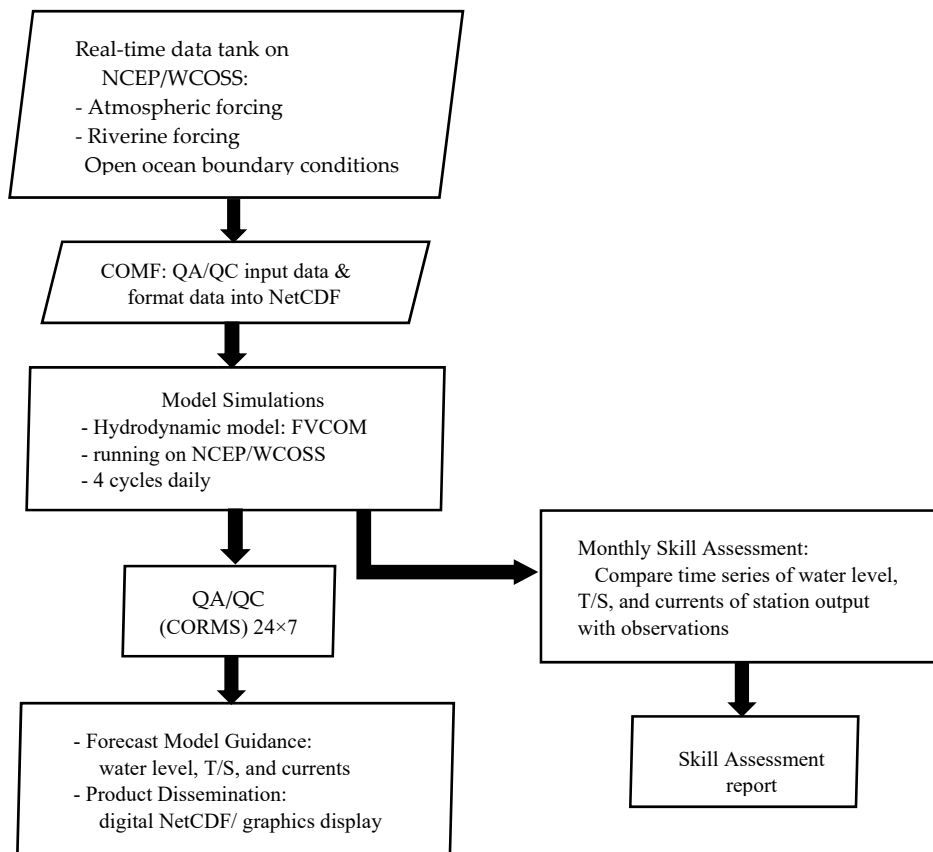


Figure 3. Conceptual structure and the operational and data analysis procedures of the NGOM operational forecast systems.

Three OFS produce six hours of nowcast, and up to 48 hours of forecast guidance, for water levels and three-dimensional currents, water temperatures, and salinity four times a day at 0300, 0900, 1500 and 2100 UTC. Both the hourly field and the 6-minute station (at locations with available observed data) NetCDF outputs are archived and disseminated at the Linux data tank (<https://opendap.cco-ops.nos.noaa.gov/netcdf/>) of the National Ocean Service (NOS). In addition, COMF generates time series plots of station outputs (24-hour nowcast and 48-hour forecast), which include water levels, currents, temperatures, salinity, and surface winds. These outputs are depicted in both contour and vector map plots. Additional graphics include the animation of water levels, currents, temperatures, salinity, and surface winds. The graphics are published through the NOS operational forecast system (OFS) webpage at (<https://tidesandcurrents.noaa.gov/ofs/ngofs/ngofs.html>). To ensure a high level of model skill, CO-OPS validates the model performance each month by comparing the time series of station outputs with observed data using the NOS skill assessment software [21], which generates model skill reports.

In recent years, the Gulf Coast user community has proposed a growing need for forecast guidance in the NGOFS areas not covered by the three existing OFS. A short list of these areas include the lower Mississippi River course, Lake Pontchartrain, various Texas coastal embayments, Mexican coastal waters, etc. (Figure 1). From an operational point of view, it is more efficient to operate and maintain one combined system, rather than three separate systems. To fulfill user needs and to foster the system’s operational efficacy, NOAA decided to combine the three existing OFS into one integrated system. The domain of this new system includes the combined domains of the three existing OFS, as well as the previously unresolved coastal embayments and river courses. Tentatively, it is named the Integrated Northern Gulf of Mexico OFS (INGOFS). Like NGOFS, INGOFS will use FVCOM as its core hydrodynamic model. It is designed to produce a real-time nowcast, and up to 48 hours of

forecast guidance for water levels, 3-D currents, water temperatures, and salinity. It is planned to begin operations in mid-2020.

This article describes technical details of the INGOFS development and model configuration, as well as the setup and verification of a one-year (2 August 2016–1 August 2017) simulation. Since the model run was for a historical period, it will be referred to as hindcast in the following. This section introduces background information including the initiative for the system development. Section 2 describes the model hindcast simulation setup. Section 3 describes the observational data used to verify the hindcast results. Section 4 presents the model results. Section 5 discusses the domain-averaged model skill of the water surface temperatures and water levels, and the impact of initial salinity conditions on the model performance. Section 6 states the summary and future plans.

2. Methods

INGOFS uses the Finite Volume Community Ocean Model (FVCOM) [17] as its core hydrodynamic model. FVCOM is an unstructured grid, finite-volume, three-dimensional, primitive equation ocean circulation model. It uses triangular grids to map the model domain in the horizontal and a terrain-following σ -coordinate in the vertical. The unstructured grid enables an accurate coastal geometric fit. FVCOM is a prognostic model; it is composed of internal and external modes which are computed separately using two split steps. The model uses a second-order finite-volume method to solve the equations of motion by the flux calculation in the integral form of primitive equations. The approach provides an ideal representation of momentum, mass, salt, and heat conservation.

The turbulence parameterization employs the modified Mellor and Yamada level-2.5 turbulence closure model [22] for vertical mixing. The Smagorinsky formulation [23] is used for horizontal mixing. FVCOM was successfully applied to studies of the deep ocean [24], the continental shelf [25], and estuaries [26,27]. A detailed description of FVCOM is available at <http://fvcom.smast.umassd.edu/FVCOM/index.html>.

The INGOFS domain encompasses broad NGOM coastal waters spanning from the coast of Mexico near (97.6° W, 21.8° N) in southwest, across the U.S. Gulf Coast in the northwest, north, and northeast, and all the way to the west of Panama City in the east (Figures 1 and 2). The domain's open ocean boundary approximates the 300-m isobaths, except near the Mississippi River mouth, where the model boundary extends further outward beyond the shelf break to a depth as great as 1700 m. Except for the portion of the grid in Mexican coastal waters, the INGOFS grid shares the same open ocean boundary as that of NGOFS.

In addition to encompassing the combined NGOFS, NWGOFS, and NEGOFs domains, the INGOFS domain also covers the Lower Mississippi River course, Lake Pontchartrain, Barataria Bay, the lower Atchafalaya River, Texas coastal inlets, and a portion of the Mexican coastal waters (Figures 1 and 2). From the perspective of grid generation, the INGOFS grid is composed of two parts: the combined NGOFS and NWGOFS/NEGOFS grid, and the newly generated grids for extended coverage. The former includes Lake Charles, Sabine-Neches, Galveston Bay, Matagorda Bay, Mobile Bay, Pascagoula, and Gulfport. Figure 2a,b shows the combined NGOFS, NWGOFS/NEGOFS grid and the INGOFS grid, respectively. Figure 4a,b displays close up views of the grids covering the Texas coastal embayments and the lower Mississippi River and adjacent waters, respectively. The INGOFS grid is composed of 303,714 nodes and 569,405 elements. For comparison with the existing OFS grids, Table 1 lists the dimensions and spatial resolution of both the existing OFS and the INGOFS grids.

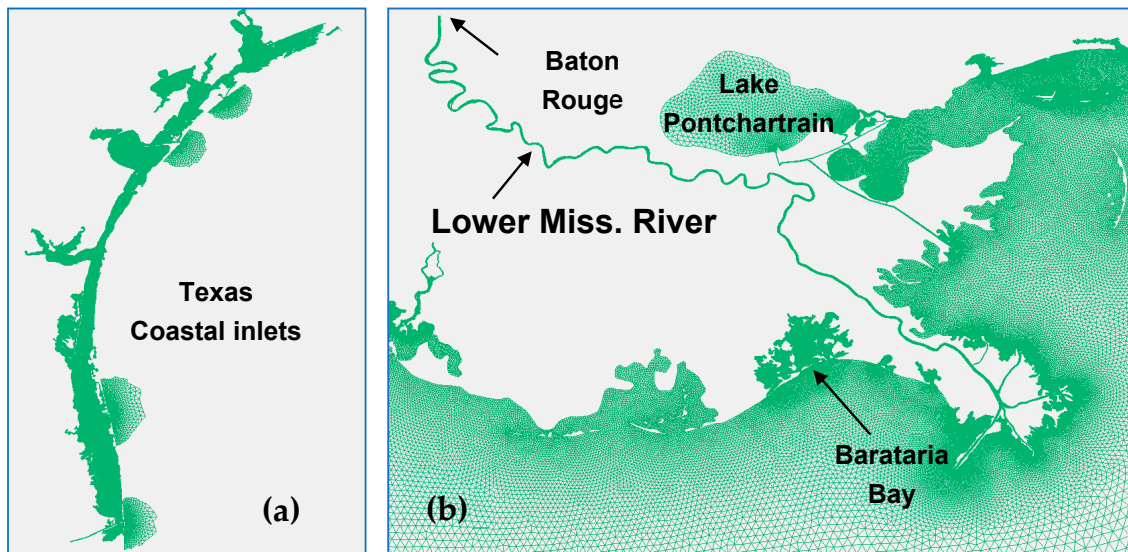


Figure 4. Close up view of the INGOFS model grid in two regions, (a) Texas coastal embayments, and (b) the lower Mississippi River course, Barataria Bay, and Lake Pontchartrain.

The INGOFS bathymetry was populated using NGOFS, NWGOFS/NEGOFS grid bathymetry, the Vertical Datum (VDatum) (<https://vdatum.noaa.gov/welcome.html>) model grid bathymetry [28], the NOAA Sounding and Electronic Chart (ENC) bathymetry, and the ADCIRC model grid bathymetry in the Western North Atlantic, Caribbean and Gulf of Mexico ADCIRC Tidal Database (EC2015) [29]. Depending on sources of the INGOFS grid generation and geographical locations, bathymetry was populated in three ways. For any portion of the grid which originated from any of the three existing OFS, the bathymetry remained to be the same as the bathymetry in the source grid. For the remaining portion of the grid in U.S. coastal waters, the bathymetry was populated by linearly interpolating the combined VDatum model grid for the Mississippi River and the New Orleans region [28], as well as the ENC and sounding bathymetry. Bathymetry of the grid covering Mexican waters was populated by linearly interpolating the EC2015 ADCIRC grid bathymetry. Figure 5 displays the color-coded bathymetry.

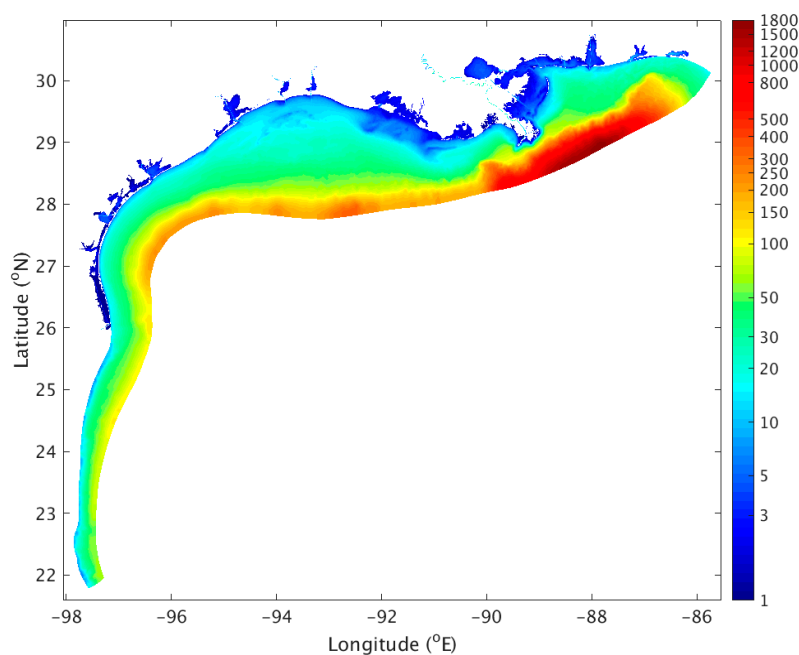


Figure 5. The INGOFS model grid bathymetry. Color bar is in meters.

Using the above model grid and bathymetry configuration, we conducted a one-year (2 August 2016–1 August 2017) hindcast simulation. The simulation was driven with the complete suite of model forcing data including open ocean boundary forcing of the combined tidal and subtidal water levels and currents. Additional model forcing included 3-dimensional temperatures (T) and salinity (S), river flows, and sea-surface meteorological forcing. The tidal water level harmonics were interpolated using the EC2015 tidal database [29]. Considering the relative importance of various tidal constituents in the model domain, we chose eight major tidal constituents, namely, luni-solar (K_1), principal lunar (O_1), principal solar (P_1), elliptical lunar (Q_1), principal lunar (M_2), principal solar (S_2), elliptical lunar (N_2), and luni-solar (K_2) to reconstruct the tidal forcing data.

The non-tidal open ocean conditions used the nowcast results from the Global Real-Time Ocean Forecast System (G-RTOFS) [30,31]. G-RTOFS is run by the National Centers for Environmental Prediction (NCEP) of NOAA. G-RTOFS makes use of the Naval Oceanographic Office’s configuration of the 1/12-degree eddy resolving global Hybrid Coordinates Ocean Model (HYCOM) as its core hydrodynamic model. The HYCOM model has horizontal dimensions of 4500 by 3298 and 32 hybrid layers (isopycnals in the deep, isolevel in the mixed layer, and sigma in shallow) in the vertical. The system assimilates in situ profiles of temperature and salinity from a variety of sources, and also assimilates remotely sensed sea-surface temperature (SST), sea-surface height (SSH), and sea-ice concentrations. It runs once a day and produces nowcast and forecast guidance for sea surface values of SSH, SST, and sea-surface salinity (SSS) at three-hour intervals. In addition, it produces full volume parameters (3-dimensional temperature, salinity, currents, and mixed layer depths) at six-hour intervals. The nowcast outputs of three-hourly water levels and six-hourly 3-D currents, temperatures (T) and salinity (S), and non-tidal forcing were spatially interpolated onto the model grid’s open ocean boundaries and temporally interpolated throughout the INGOFS hindcast period.

The river forcing used discharge from 29 rivers along the INGOFS land boundary. Table 2 lists the USGS station identifications (IDs) and station names. Some big rivers, with wide cross sections, were resolved through multiple grid nodes. In such cases, river discharge was evenly distributed across the nodes. Discharge from the 29 rivers is distributed over 63 model nodes. Figure 6 shows the river node locations.

Table 2. USGS river station IDs and names.

No.	IDs	Station Names	No.	IDs	Station Names
1	2365500	Chocta Whatchee River at Caryville, FL	16	8015500	Calcasieu River Near Kinder, LA
2	2368000	Yellow River at Milligan, FL	17	8030500	Sabine Rv Nr Ruliff, TX
3	2375500	Escambia River Near Century, FL	18	8041780	Neches Rv Saltwater Barrier at Beaumont, TX
4	2376500	Perdido River at Barrineau Park, FL	19	8066500	Trinity Rv at Romayor, TX
5	2470629	Mobile River Near Landon, MS	20	8069000	Cypress Ck Nr Westfield, TX
6	2471019	Tensaw River Near Mount Vernon, AL	21	8075000	Brays Bayou at Houston, TX
7	2479000	Pascagoula River at Merrill, MS	22	8075400	Sims Bayou at Hiram Clarke St, Houston, TX
8	2479560	Escatawpa River Near Agricola, MS	23	8076000	Greens Bayou Nr Houston, TX
9	2481510	Wolf Rv Nr Landon, MS	24	8116650	Brazos Rv Nr Rosharon, TX
10	2489500	Pearl River Near Bogalusa, LA	25	8162500	Colorado Rv Nr Bay City, TX
11	2492000	Bogue Chitto River Near Bush, LA	26	8164000	Lavaca Rv Nr Edna, TX
12	7374000	Mississippi River at Baton Rouge, LA	27	8164800	Placedo Ck Nr Placedo, TX
13	7375500	Tangipahoa River at Robert, LA	28	8188800	Guadalupe Rv Nr Tivoli, TX
14	7381600	Lower atchafalaya River at Morgan City, LA	29	8211200	Nueces Rv at Bluntzer, TX
15	8012000	Nezperque Near Basile, LA			

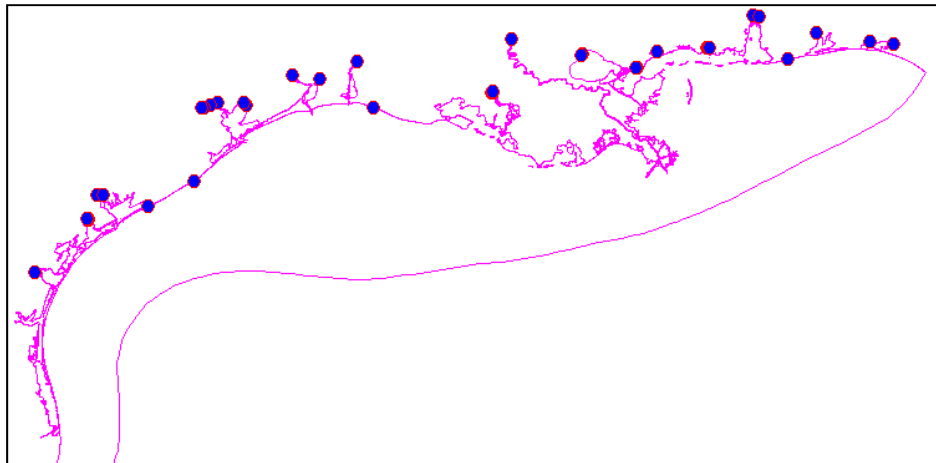


Figure 6. River forcing locations on the INGOFS grid. Discharges of the 18 rivers total are distributed across 63 grid nodes.

The river flow data were from the U.S. Geological Survey (USGS) river discharge observations [32]. It is noted that not all USGS river discharge measurements were accompanied by simultaneous water temperature measurements. For the stations without temperature data, the temperature measurements from nearby Center for Operational Oceanographic Products and Services (CO-OPS) stations were used. The salinity was specified to be zero for all 29 rivers.

The hindcast made use of the 6-km resolution forecast guidance from the NOAA National Centers for Environmental Prediction's (NCEP's) North American Mesoscale Forecast Modeling System (NAM) for surface forcing. The INGOFS hindcast was forced with 10-m wind velocity to compute the surface wind stress, and with 2-m surface air temperature and relative humidity. Additional forcing included the total shortwave radiation, downward longwave radiation, the FVCOM bulk formulation to calculate the air-sea momentum, and the Coupled Ocean–Atmosphere Response Experiment (COARE) algorithm [33] to compute heat flux across the air-sea interface.

The hindcast simulation ran from 2 August 2016 to 1 August 2017. It started from a still water state with the water temperature and salinity fields initialized with combined INGOFS, NWGOFS/NEGOFS outputs. The model was configured in 20 sigma layers. It used the FVCOM wetting and drying feature, the quadratic bottom friction scheme, and the two-equation model of the Mellor–Yamada Level 2.5 turbulence closure scheme. The internal model time step was 9 s and the external to internal time step split ratio was equal to 3.

3. Observational Data

The observational data used to verify the model results included water level time series from the National Ocean Service (NOS) CO-OPS water level stations. Temperature data (T) and salinity data (S) from CO-OPS meteorological observation stations, and temperature data from National Data Buoy Center (NDBC) buoys were also included. The water level data were downloaded via the CO-OPS online archive [34]. Table A1 lists the station IDs, names, and station location information.

The T and S data collected from either the CO-OPS or NDBC buoys were downloaded through the NDBC online archive [35]. The observation depths ranged between 0.5 m and 3 m beneath the sea surface.

Please note that every CO-OPS station possesses dual station IDs—one in the CO-OPS naming convention and one in the NDBC naming convention. To be clear, the stations are hereafter referred to only by their NDBC IDs. Tables 3 and A2 show the station IDs, names, and geographical information for temperature and salinity, respectively.

Table 3. Station meta data of surface salinity observations.

No.	IDs	Station Names	Longitude (°E)	Latitude (°N)
1	42067	USM3M02	−88.649	30.043
2	BSCA1	Bon Secour, AL	−87.829	30.329
3	CRTA1	Cedar Point, AL	−88.14	30.308
4	PHA1	Dauphin Island, AL	−88.078	30.251
5	KATA1	Katrina Cut, Al	−88.213	30.258
6	BLA1	Middle Bay Lighthouse, AL	−88.011	30.437
7	HPA1	Meaher Park, AL	−87.936	30.667

4. Results of Hindcast Simulations

Following an initial 6-day ramping up of both water level and velocity forcing on the open ocean boundary, the hindcast model run (Section 2) continued for another 9 days to ensure that an equilibrium state was reached. The time series of water levels, temperatures and salinity were recorded at 6-minute intervals from the 15th day to the end of the hindcast simulation. We then verified the model results by comparing the model time series outputs with the observed time series (Section 3). We calculated root-mean-square errors (RMSE) of water levels, sea-surface temperatures (SST), and salinity (SSS).

4.1. Water Level

Figure 7a–d shows both the model (red lines) and the observed (blue lines) total water level times series at stations 8735391, 8761927, 8771013, and 8775792. The station sites span from the Texas coastal inlets in the western model domain to Galveston Bay, Texas, Lake Pontchartrain, and Mobile Bay in the eastern domain. They were selected to roughly represent the model performance in various areas across the Gulf Coast domain. For clarity of display, only two months (1 September through 1 November 2016) of the entire 1-year comparison are displayed. The model and data exhibit favorable agreement in both tidal and subtidal frequencies. The RMSE at the four stations were 7.9 cm, 8.1 cm, 8.5 cm, and 7.6 cm, respectively.

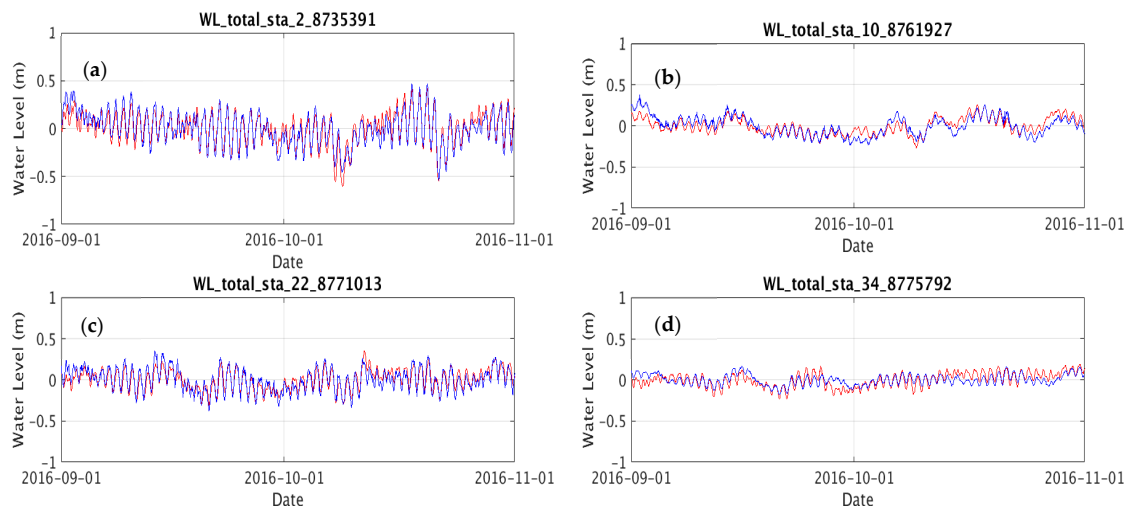


Figure 7. Comparison of model (red lines) and observed (blue lines) water levels at CO-OPS water level stations (a) 8735391, (b) 8761927, (c) 8771013, and (d) 8775792. See the station locations in Figure 1.

To investigate the model performance on the subtidal water levels, total water level time series were low-pass filtered with a 30-day Fourier Transform low-pass filter. Figure 8a–d shows the model and observed subtidal time series between August 15, 2016 and August 1, 2017 at the same four stations as shown in Figure 7. The hindcast simulation successfully reproduced the observations in both time and magnitude during both eventful and uneventful periods. For instance, it accurately reproduced the water level setup in mid-June 2017 at stations 8735391 and 8761927 (Figures 7 and 8) and setdown

near the end of January 2017 at station 8771013. During quiescent periods such as September through November 2017, the model results also demonstrate favorable agreement with observations at all four stations. The model RMSEs at the four stations were 6.8 cm, 7.7 cm, 6.9 cm, and 7.2 cm, respectively.

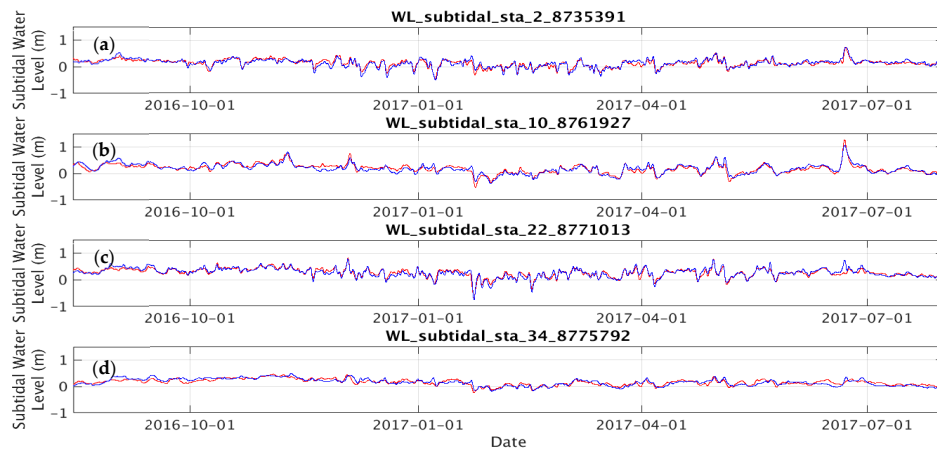


Figure 8. Comparison of model (red lines) and observed (blue lines) water levels at CO-OPS water level stations (a) 8735391, (b) 8761927, (c) 8771013, and (d) 8775792. See the station locations in Figure 1.

Figure 9a,b illustrates the RMSE maps of the total and subtidal model water levels at 55 CO-OPS water level stations (Table A1). In general, RMSE is evenly distributed across the model domain, except for stations 8760721 and 8761955 along the lower Mississippi River. Comparing the model-data water level time series in addition to the Mississippi River discharge measured at USGS station 07374000 (Baton Rouge, LA) (Table 2), it has been identified that the larger RMSE can be attributed to the water level setup from a large river discharge event which occurred between May and June of 2017. The river discharge during this period reached a magnitude as large as about 36,400 m³/s as compared with an average value of about one-third of that value during the remaining time of the hindcast period. Not including the two Mississippi River stations, the average total water level RMSE equals about 8.6 cm with a standard deviation (SD) of 1.8 cm, and the average subtidal RMSE equals about 7.4 cm with a SD of 1.7 cm.

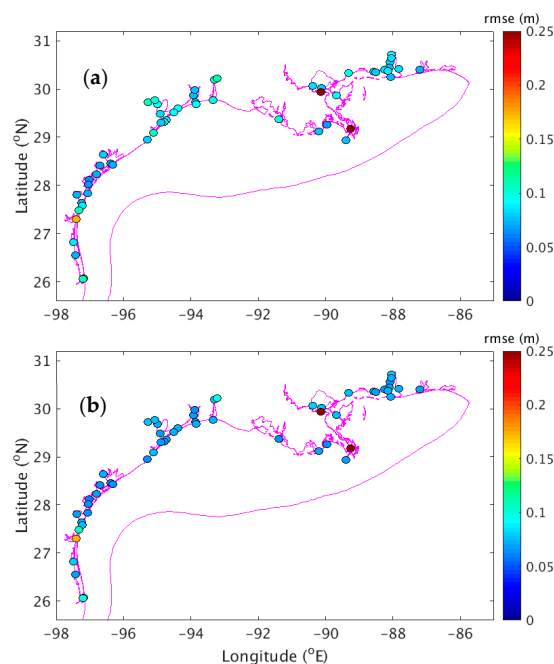


Figure 9. The RMSE of the model (a) total water levels and (b) subtidal water levels at 55 CO-OPS stations (Section 4.1).

The monthly mean RMSE and absolute values of the model-data differences ($|bias|$) of the modeled total water levels at each station were averaged over the 53 stations out of the total 55 stations (Table A1). The two Mississippi River stations, 8760721 and 8761955, were deemed to be outliers, and hence, were excluded. Figure 10a,b shows the RMSE and $|bias|$, respectively. The RMSE ranges between 0.06 cm and 0.11 cm and the $|bias|$ ranged between 0.01 m and 0.06 m. Neither of the two properties exhibited significant seasonal variability.

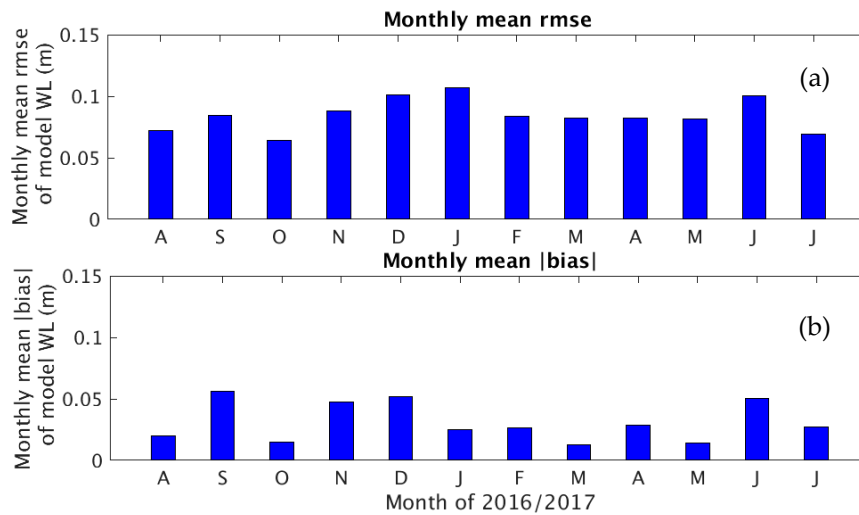


Figure 10. Monthly means of (a) the root-mean-square errors (RMSE) and (b) absolute model-data differences ($|bias|$) of the hindcast total water level.

Figure 11 illustrates the pattern match between the model results and the observations in a Taylor Diagram [36]. In general, a Taylor Diagram provides a graphical framework that allows a suite of modeled variables to be compared with observed data. The model-data correlation coefficient (COR) and the standard deviation (SD) of both the modeled and observed data from each station were calculated using the time series data described in the above. The magnitude of both the SD and the RMSE vary across the range of stations. To eliminate the factor of station variability, the normalized SD (nSD) and the normalized RMSE (nRMSE) were calculated by dividing the model SD and RMSE by the SD of the observed data. The nRMSE measures the ratio of the model RMSE to the SD of the observed data. When shown in the Taylor Diagram, modeled patterns that agree well with observations will lie nearest to the line of nSD equal to 1 [37].

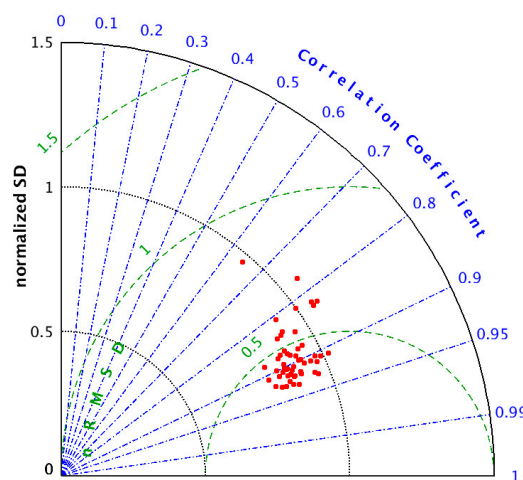


Figure 11. The Taylor Diagram of water level. Shown on the plot are the model-data correlation coefficient, normalized SD and normalized RMSE (nRMSE).

Shown in Figure 11 are the model-data COR, the nSD, and the nRMSE. The majority of data points lie close to the line of nSD equal to 1. This indicates that most of the stations demonstrate a rather favorable pattern match between the model results and the observations. The model results and observed data are highly correlated; the averaged COR equals to 0.91. With the exception of one outlier station (ID 8776139) with a COR equal to 0.49, the COR ranges from 0.76 to 0.94 with an average of 0.88; the nSD ranges between 0.79 and 1.07 with an average of 0.91; and the nRMSE ranges between 0.36 and 0.99 with an average equal to 0.45.

4.2. Sea-Surface Temperature (SST)

Figure 12 illustrates the monthly model mean and observed mean SST at stations 42012, MCGA1, NWCL1, PILL1, MGPT2, and PMNT2, respectively. From top to bottom, the stations are located in the open coastal area southeast of Mobile Bay, Lake Pontchartrain, the lower Mississippi River, Galveston Bay, and the Texas coastal embayments. They were chosen to investigate model performance in both the offshore and in embayment areas. In the figure, the left panel illustrates monthly average SST of model (red bars) and observations (blue bars), as well as the standard deviation of each data set. The right panel illustrates the corresponding monthly averaged model bias in terms of model-data difference for each month.

In general, the hindcast simulation successfully captured seasonal cycles in SST and demonstrated favorable agreement with observations. Both model and observed SST demonstrate significant seasonal variability, with SST ranging from about 9 °C in the winter season to about 32 °C in the summer season. The model bias ranges between −1.8 °C and 1.7 °C. In the summer season, the model over predicted SST, whereas in the winter season it over predicted SST at the open coastal station (42012) and at the lower Mississippi River station (PILL1) and underpredicted SST at the other embayment stations.

Figure 13 displays the color-coded RMSE at 52 stations (Table A2). The RMSE ranges from 0.6 °C to around 2.1 °C. In general, the model demonstrates better skills, with RMSE less than 0.8 °C, in the offshore areas as opposed to nearshore embayments. Compared with the relatively deeper offshore areas, the embayments usually experience far more sophisticated ambient conditions, such as large river discharge and significant diurnal cycles in the surface forcing. Therefore, it is far more challenging to accurately reproduce the SST field in coastal embayments than in offshore areas.

Figure 14a,b shows the RMSE and the absolute average of the model-data differences, respectively. The RMSE ranged between 0.7 °C and 1.5 °C, and the bias ranged between −0.3 °C and 0.2 °C. The maximum RMSE appeared between December 2016 and January 2017. This indicates that the model was least satisfactory in reproducing the winter season SST. In general, the bias was positive between August and December, 2016 and negative between January and July, 2017. The SST was slightly overpredicted during the former period and underpredicted during the latter.

Figure 15 shows the Taylor Diagram to illustrate the model-data COR, the normalized standard deviation (nSD), and the normalized RMSE (nRMSE). The three parameters were calculated using the same method as described for water levels in Section 4.1. The majority of data points lie close to the line of nSD equal 1. This indicates that most of the stations demonstrate rather favorable pattern match between the model results and the observations. The model results and observed data are highly correlated; the averaged COR equals to 0.95. With the exception of one station (ID 42067) with a COR equal to 0.77, the COR ranges between 0.93 and 1.0 with an average of 0.98; nSD ranges between 0.81 and 1.24 with an average of 0.99; nRMSE ranges between 0.17 and 0.27 with an average equal to 0.21.

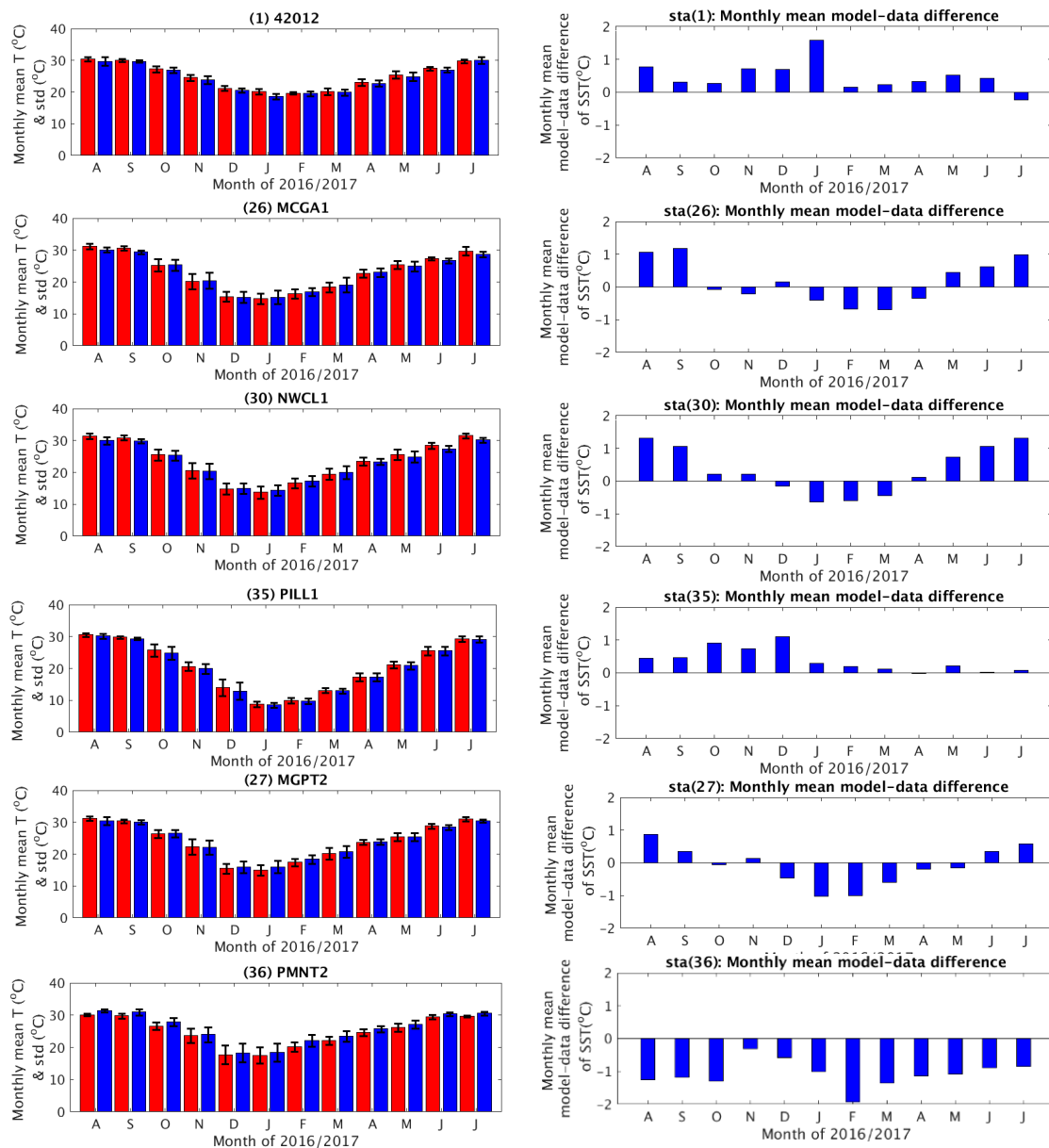


Figure 12. Left panel—Comparison of monthly model output mean SST (red bars), and monthly observed mean SST (blue bars), and the standard deviation of each data set. Right panel—monthly mean model bias. The station IDs are shown in the title of each plot. See the station locations in Figure 1.

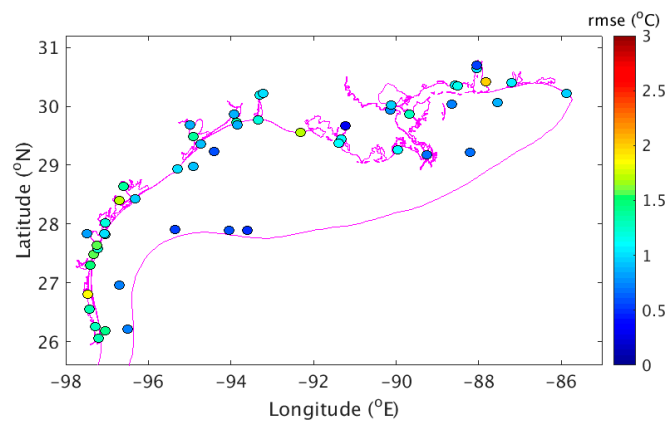


Figure 13. Color-coded RMSE of the modeled SST at 52 stations (Table A2).

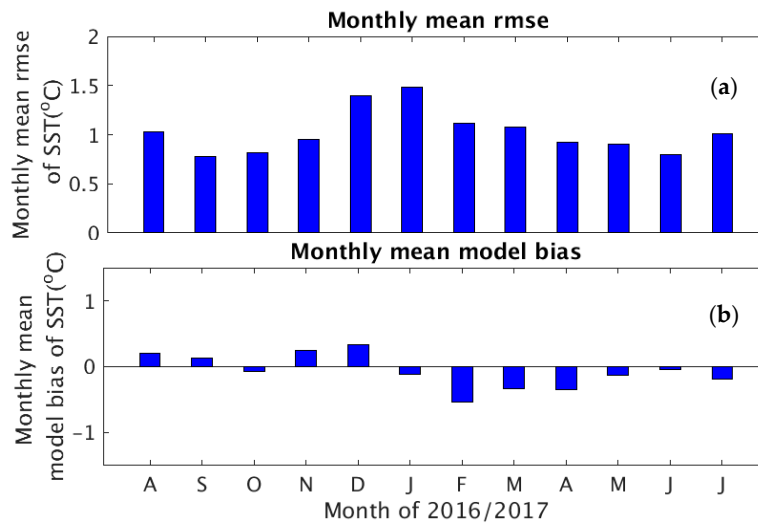


Figure 14. Monthly mean (a) RMSE and (b) the absolute model-date differences of the hindcast SST.

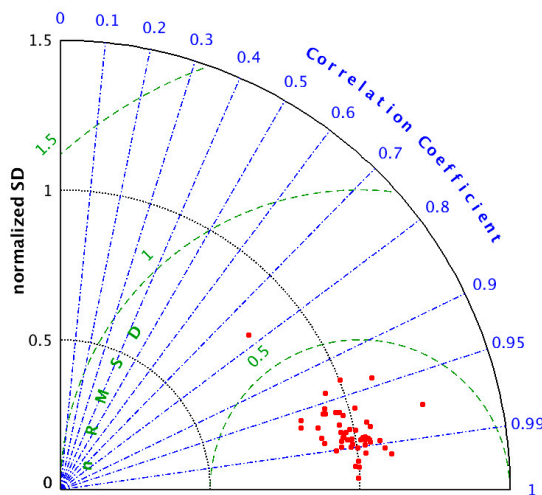


Figure 15. The Taylor Diagram of the sea-surface temperature. Shown on the plot are the model-data correlation coefficient, normalized SD (nSD) and normalized RMSE (nRMSE).

4.3. Sea-Surface Salinity (SSS)

During the hindcast period, salinity observations were available at seven stations (Table 3). All seven stations are situated either inside or close to Mobile Bay that represents a rather small area of the entire INGOFS domain. Station 42067 is situated offshore, southwest of the MB. Stations BSCA1, CRTA1, DPHA1, and KATA1 are located in the lower MB, while stations MBLA1 and MHPA1 are located in the mid- and upper MB, respectively.

The malfunction of salinity sensors by bio-fouling is very common in coastal areas of the northern gulf of Mexico [18]. Many observed data were easily deemed to be false measurements due to the malfunction of salinity sensors. Figure 16a,b showed the SSS time series at stations CRTA1 and DPHA1, respectively. To point out a few problematic data points, SSS exhibited a nearly 10 psu change within a one-hour period in 14 March 2017 or a nearly 20 psu daily change in 10 April 2017.

Considering the geographical limitation of the station locations and the data quality of observations, it is noted that the hereafter presented model-data comparison results were far from being representative from the perspective of obtaining an objective assessment of the model skill assessment for the entire domain.

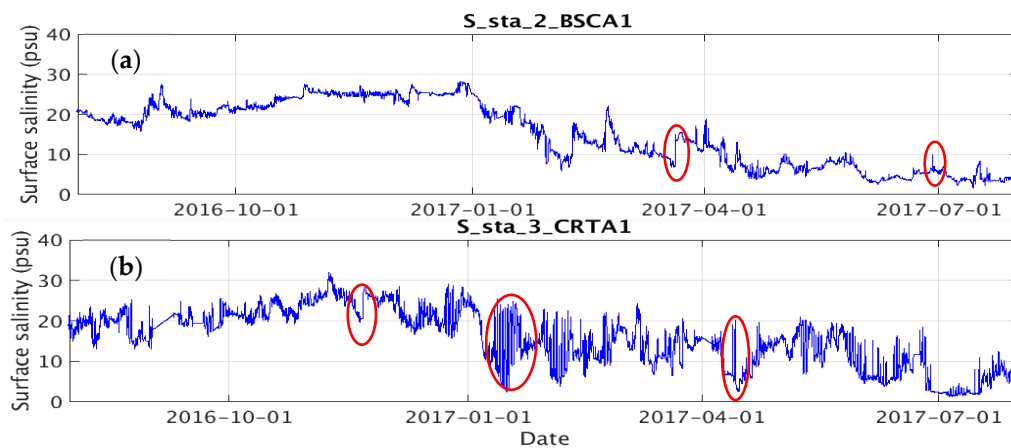


Figure 16. The observed surface salinity time series at stations (a) BSCA1 and (b) CRTA1. Red ellipses marked occurrences the sensor false measurements.

Figure 17 illustrates the comparison of monthly mean SSS between the modeled and observed SSS at the seven stations. The inset of Figure 1 shows the station locations. The left panel shows the model (red bars) and observed (blue bars) monthly means, as well as the standard deviation of each data set. The modeled and observed SSS exhibited similar seasonal variability. In general, SSS gradually increased from summer of 2016 and peaked at nearly 32 psu in the winter of 2016. As the time gradually approached the summer of 2017, SSS dropped to 5–13 psu in the mid-bay area (station MBLA1) and even reached nearly zero psu at the upper bay station MHPA1. The monthly averaged model bias ranged from -6 psu to 6 psu. The yearly mean model RMSE at each station was, respectively, 2.6, 3.7, 3.8, 5.4, 4.9, 3.0, and 2.7 psu.

The right panel shows the monthly mean absolute model-data differences. The model skill was least satisfactory in the winter season of the year. The model bias ranged from about 2 psu in February 2017 to 2.1 psu in January 2017, with a yearly average of 0.7 psu. The model overpredicted SSS between February and April of 2017 and overpredicted SSS in the remaining hindcast period.

It is noted that the initial salinity condition of the hindcast runs was populated with the combined NGOFS and NWGOFS/NEGOFS outputs (Section 1). In addition, we tested running hindcast simulations using the initial conditions populated with the G-RTOFS salinity field. The G-RTOFS domain did not cover small coastal embayments such as Mobile Bay, etc. Hence, the INGOFS salinity field in the area was extrapolated from nearby G-RTOFS offshore model grid points outside of the embayments. This naturally caused the INGOFS initial salinity fields in the embayments to be much more saline than observations and may produce a large model-data discrepancy.

We compared the modeled time series from the two different initial conditions with observations at six stations (Table 3). Figure 18a–d shows the surface-salinity fields at the upper bay station MHPA1, at mid-bay stations MBLA1 and BSCA1, and at the offshore station 42067. They represent the upper, mid-bay, lower, and offshore stations, respectively. It was found that the impact of initial conditions may persist as long as two and a half months (until mid-October 2016) in the upper and lower bay region, nearly three months (until the beginning of November 2016) at the upper-bay station, and about one and a half months at the offshore station. After the initial one to two months, the two salinity time series gradually converge, and the impact of the initial condition difference becomes insignificant.

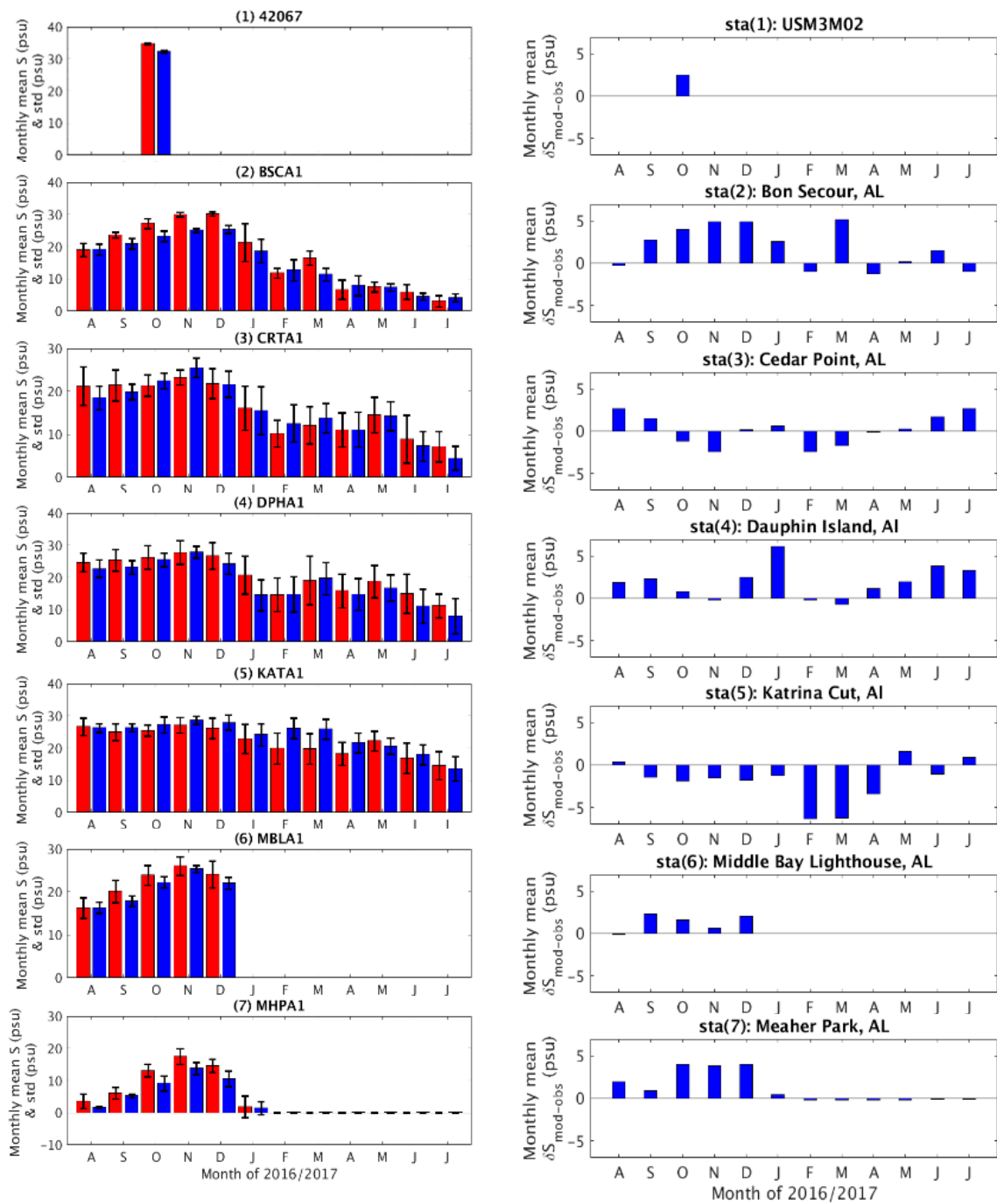


Figure 17. Comparison of monthly mean SSS between the hindcast results and observation, (left panel) monthly mean SSS of model (red bars), observations (blue bars), and the standard deviation of each data set and (right panel) monthly mean model bias. The station IDs are shown in the title of each plot. See the station locations in Figure 1.

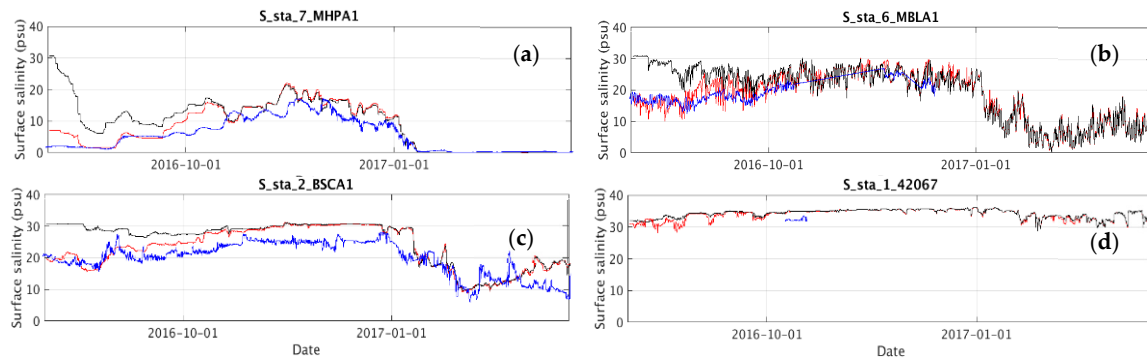


Figure 18. Comparison of the observed (blue lines) and the hindcast (black and red lines) salinity time series at stations (a) MHPA1, (b) MBLA1 and (c) BSCA1, and (d) 42067. The two model time series correspond to initial salinity conditions populated with G-RTOFS (black lines) and NGOFS (red lines), respectively.

5. Discussion

5.1. Comparison of Model Skills with Other OFS

This section compares the model performance of water levels (WL) and sea-surface temperatures (SST) between the INGOFS and the NGOFS/NWGOFS/NEGOFS (hereafter referred to as NGOFS for simplicity of description). Figure 19a shows the comparison of the water level RMSE in a scatter plot, while Figure 19b shows the map of the RMSE differences between INGOFS and NGOFS at 28 stations. Similarly, Figure 20a,b shows the SST comparison between INGOFS and NGOFS at 26 stations. The RMSE of INGOFS was calculated based on the hindcast results described in Section 4. The RMSE of NGOFS was taken from previous publications on the NGOFS development and model skill [18,19]. It was calculated based on hindcast simulations from different time periods from those of the INGOFS; however, since the results were objective and representative of NGOFS model skill, it is valid to compare the two RMSE data sets. Interested readers are recommended to reference the above publications for technical details. To conduct the comparison, we identified the stations used in both the INGOFS and NGOFS skill evaluations and compared the RMSE between INGOFS and NGOFS. There are no salinity stations shared between INGOFS and NGOFS and hence, comparison of salinity is omitted in the present discussion.

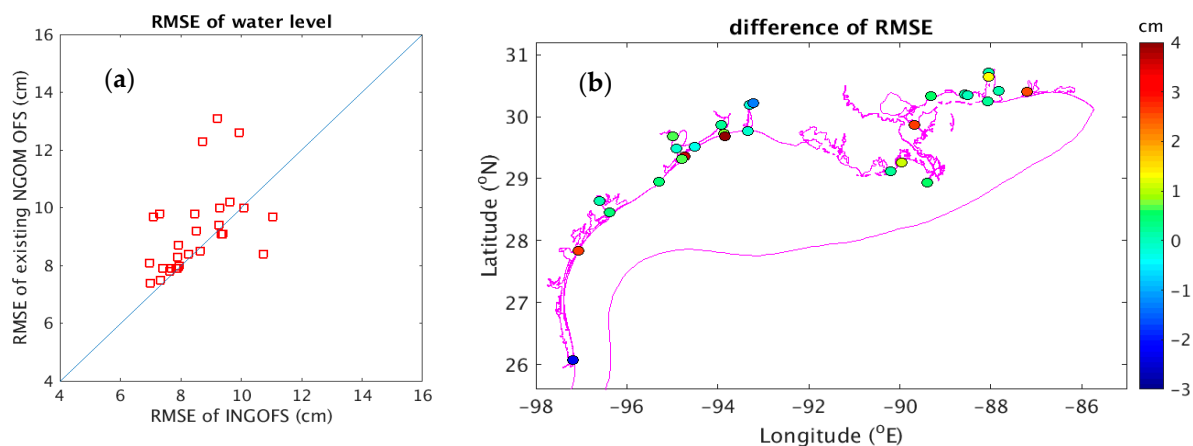


Figure 19. Comparison of the water level skill between the INGOFS and the NGOFS, (a) scatter plot of RMSE and (b) the RMSE difference between INGOFS and NGOFS.

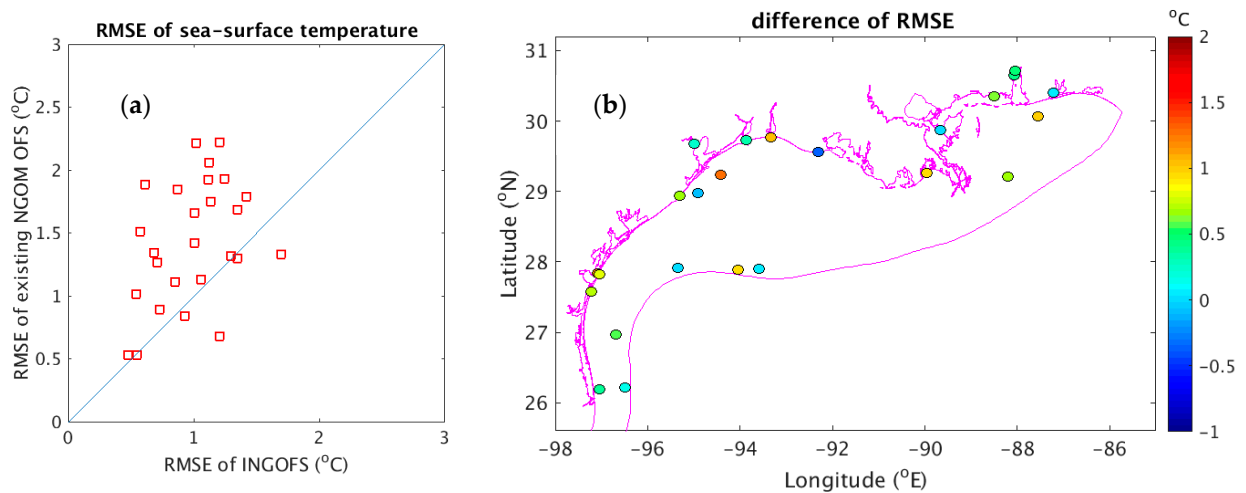


Figure 20. Comparison of the SST skill between the INGOFS and the NGOFS, (a) scatter plot of RMSE and (b) the RMSE difference between INGOFS and NGOFS.

INGOFS demonstrates slightly better model skill than does NGOFS for both water levels and sea-surface temperatures (Figures 19 and 20). For water levels, INGOFS exhibits slightly smaller RMSE than NGOFS. The INGOFS RMSE ranges between 7.0 cm and 11.0 cm, whereas the NGOFS RMSE ranges between 7.4 cm and 13.1 cm. The RMSE difference between INGOFS and NGOFS ranges from -3.9 cm to 2.3 cm, and the average of the differences over all 28 stations is about -0.6 cm. For SST, the RMSE of INGOFS ranges between 0.5 °C and 1.7 °C, while the RMSE of NGOFS ranges between 0.5 °C and 2.2 °C. The RMSE difference between the two ranges from -0.5 °C to 1.3 °C, and the average of the differences over all 26 stations is 0.4 °C.

5.2. Limitation of the RMSE Analysis

The RMSE has its limitation as a statistical parameter in terms of objectively representing the model errors. It is based on averaged squared differences and hence tends to be insensitive to lower magnitude events and biased towards higher magnitude events [38–40]. However, the present discussions of the INGOFS performance (Section 4) are focused on using the RMSE. Hence, the model skill results are not entirely comprehensive. Statistical indices to differentiate low, medium, and high data values may assess the model performance more effectively [38–40]. This method will be applied in future assessments of the INGOFS performance and is expected to give a more comprehensive and objective depiction of the model skill.

In the following, we show results from a preliminary investigation on the distribution of the RMSE values. We calculate occurrence frequency (F) and cumulative frequency (CF) of various RMSE values over the entire time series (Section 4). To estimate F and CF, the absolute value of each point in the model-data difference time series was calculated for all stations (Tables A1 and A2). We then blended the data points into one data set and sorted the data into multiple bins according to their magnitudes and estimated the frequency and cumulative frequency of the data occurrence in each bin. The RMSE of the data points in each bin was then estimated. Figure 21a,b displays F and CF of the RMSE for water level and SST, respectively. In each plot, the abscissa corresponds to the central value of each RMSE bin, whereas the bar charts (blue) and the curve (orange) represent F and CF, respectively. The bin width is 0.02 m for water levels and 0.1 °C for the SST. Both water levels and SST demonstrate similar characteristics for F and CF. Both F and CF decrease drastically in a monotonic manner with the increasing RMSE. This indicates that greater model RMSEs account for a much smaller portion of the total occurrence than the smaller values. For water levels, the RMSE values less than 0.15 m accounts for over 80% of the total occurrence. For SST, the RMSE values less than 2 °C accounts for about 90% of the total occurrence.

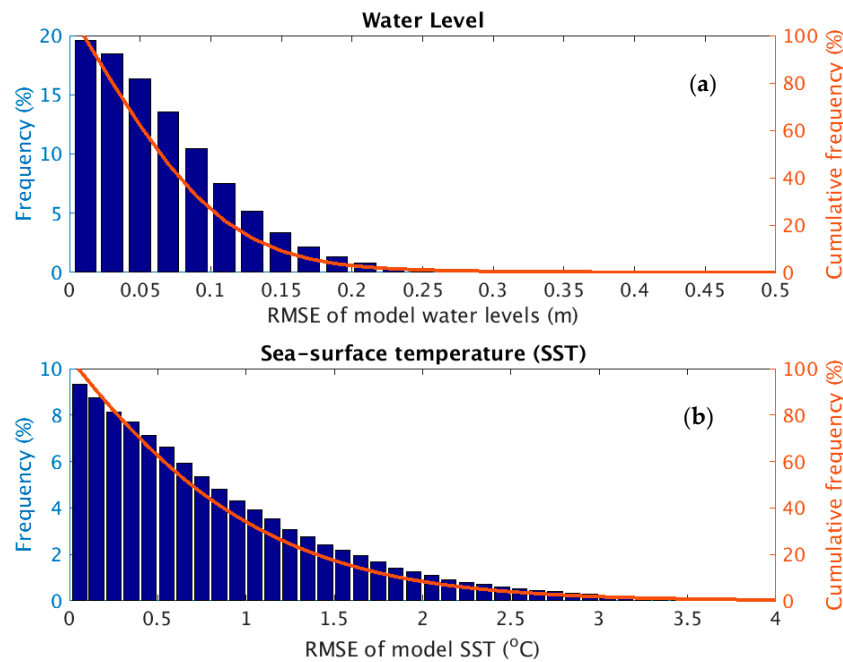


Figure 21. Frequency and cumulative frequency of the model RMSE for (a) the water levels and (b) the sea-surface temperatures.

6. Summary and Conclusions

NOAA’s National Ocean Service (NOS) is upgrading the northern Gulf of Mexico (GOM) operational nowcast/forecast system (NGOFS) by integrating the three existing operational systems, NGOFS, NEGOFs, and NWGOFS, into a single system. The new system will have extended domain coverage to encompass the lower Mississippi River, Lake Pontchartrain, Texas coastal embayments, and the coast of Mexico. It is aimed to produce real-time nowcasts and short-range forecast guidance for water levels, 3-dimensional currents, water temperatures, and salinity over the continental shelf in the northern Gulf region, the adjacent coastal estuaries, and the lower Mississippi River. Upon completion, the system will support marine navigation, emergency response, environmental management, and harmful algal bloom (HAB) forecasts. This paper described the hydrodynamic model development, configuration and verification of a one-year hindcast simulation (August 2016–July 2017).

The upgraded NGOFS will be implemented using the Finite Volume Community Ocean Model (FVCOM). The system domain includes the northern GOM continental shelf from north of Cabo Rojo, Mexico in the southwest all the way to Panama City, FL in the northeast. The model grid is composed of about 300,000 nodes, 600,000 elements, and has a spatial resolution ranging from 45 m near the coast to around 10 km on the open ocean boundary.

The hindcast forcing data included atmospheric forecast guidance from the NOAA/NWS North American Mesoscale (NAM) numerical weather prediction modeling system, river discharge observations from U.S. Geological Survey gauges, and open ocean boundary conditions derived from the NWS Global Real-Time Operational Forecast System (G-RTOFS) and the ADCIRC EC2015 tidal database. The hindcast performance of water levels, temperatures, and salinity were verified by comparing the modeled and observed time series. The RMSE was 7.4 cm for water level, 1.1 °C for water surface temperatures, and 3.7 psu for surface salinity. The relatively large RMSE for salinity was partially attributed to quality issues of the observational data due to the sensor malfunction. In addition, the model-data comparison for salinity was limited to seven stations in Mobile Bay and adjacent waters. Hence the results were far less satisfactory to represent the model skill throughout the entire system domain.

For next steps, the development team will conduct systematic skill assessment on the hindcast results of water level, currents, temperatures and salinity using the standard NOS skill assessment

software [21]. Leading up to the completion of the model development, the upgraded NGOFS will be further tested in a nowcast/forecast environment for about a one-year period. It is anticipated to be in operational production on NWS’s NCEP Weather and Climate Operational Supercomputing System (WCOSS) in mid-2020.

Author Contributions: All the authors contributed to the system development. Z.Y. and Lianyuan conducted the hindcast simulation and the model result verification.

Acknowledgments: Changsheng Chen and Jianhua Qi at the University of Massachusetts provided valuable comments on the system development and hands-on help on the hindcast FVCOM model configurations. Two anonymous reviewers provided insightful comments and suggestions that substantially improved this paper. The authors would like to express our sincere gratitude to their help.

Conflicts of Interest: The authors declare no conflicts of interest.

Appendix A

Table A1. Station meta data of water level observations.

No.	IDs	Station Names	Longitude (°E)	Latitude (°N)
1	8735180	Dauphin Island	−88.075	30.25
2	8735391	Dog River Bridge	−88.088	30.5652
3	8735523	East Fowl River, Hwy 193 Bridge	−88.1139	30.4437
4	8741533	Pascagoula NOAA Lab, MS	−88.5667	30.3583
5	8747437	St. Louis Bayentrance	−89.3258	30.3264
6	8760721	Pilot Town	−89.2583	29.1783
7	8760922	Pilots Station E, SW Pass, LA	−89.4067	28.9317
8	8761305	Shell Beach, Lake Borgne	−89.6732	29.8681
9	8761724	East Point, Grand Isle	−89.9567	29.2633
10	8761927	New Canal USCG station, Lake Pontchartrain	−90.1134	30.0272
11	8762483	I-10 Bonnet Carre Floodway, TX	−90.39	30.0683
12	8764314	Eugene Island, North of Atchafalaya Bay	−91.3839	29.3675
13	8767961	Bulk Terminal	−93.3007	30.1903
14	8768094	Calcasieu Pass	−93.3429	29.7682
15	8770475	Port Arthur	−93.93	29.8667
16	8770570	Sabine Pass	−93.8701	29.7284
17	8770613	Morgans Point, Barbours Cut	−94.985	29.6817
18	8770808	High Island, ICWW	−94.3903	29.5947
19	8770822	Texas Point, Sabine Pass	−93.8418	29.6893
20	8770971	Rollover Pass	−94.5133	29.515
21	8771013	Eagle Point	−94.9183	29.48
22	8771341	Galveston Bay Entrance, TX	−94.7248	29.3573
23	8771450	GALVESTON, Galveston Channel	−94.7933	29.31
24	8771486	Galveston Railroad Bridge, TX	−94.8967	29.3017
25	8771972	San Luis Pass	−95.1133	29.095
26	8773259	Port Lavaca, TX	−96.6094	28.6403
27	8773701	Port O’Connor, Matagorda Bay	−96.3883	28.4517
28	8773767	Maragorda Bay Entrance Channel, TX	−96.3283	28.4267
29	8774513	Copano Bay, TX, TCOON	−97.0217	28.1183
30	8774770	Rockport, TX	−97.0467	28.0217
31	8775237	Port Aransas, TX	−97.0733	27.8383
32	8775296	USS Lexington, TX	−97.39	27.8117
33	8775792	Packery Channel	−97.2367	27.6333
34	8775870	Corpus Christi	−97.2167	27.58
35	8776139	S. BirdIsland, TX	−97.3217	27.48
36	8776604	Baffin Bay, TX	−97.405	27.295
37	8777812	Rincon Del San Jose, TX	−97.4917	26.825
38	8779748	South Padre Island, TX	−97.1767	26.0767
39	8779770	Port Isabel	−97.215	26.06
40	8778490	Port Mans Field, TX	−97.4217	26.555
41	8774230	Aransas Wildlife Refuge	−96.795	28.2283
42	8773037	Seadrift TCOON, TX	−96.7117	28.4083
43	8772447	USCG Freeport, TX	−95.3017	28.9433
44	8770777	Manchester, Houston Ship Channel	−95.2658	29.7263
45	8770733	Lynchburg Landing, San Jacinto River	−95.0783	29.765
46	8770520	Rainbow Bridge	−93.8817	29.98
47	8767816	Lake Charles	−93.2217	30.2236
48	8762075	Port Fourchon	−90.1993	29.1142
49	8741041	Dock E, Port of Pascagoula	−88.5054	30.3477
50	8739803	Bayou LaBatre Bridge	−88.2477	30.4057
51	8738043	West Fowl River, Hwy 188 bridge	−88.1586	30.3766
52	8737048	MOBILE, Mobile River, State Dock	−88.0433	30.7083
53	8736897	Coast Guard Sector Mobile	−88.0583	30.6483
54	8732828	Weeks Bay, AL	−87.825	30.4167
55	8729840	Pensacola	−87.2111	30.4044

Table A2. Station meta data of water surface temperature observations.

No.	IDs	Station Names	Longitude (°E)	Latitude (°N)	Model-Data Difference (°C)
1	42012	44 NM SE of Mobile, Al	-87.555	30.065	0.48
2	42019	60 nm South of Freeport, TX	-95.353	27.913	-0.23
3	42020	60 nm SSE of Corpus Christi, TX	-96.694	26.968	-0.01
4	42035	22 nm East of Galveston, TX	-94.413	29.232	0.17
5	42040	64 NM South of Dauphin Island, Al	-88.207	29.212	-0.21
6	42043	GA-252 TABS B	-94.919	28.982	0.51
7	42044	PS-1126 TABS J	-97.051	26.191	0.77
8	42045	PI-745 TABS K	-96.5	26.217	-0.08
9	42046	HI-A595 TABS N	-94.037	27.89	-0.27
10	42047	HI-A389 TABS V	-93.597	27.897	-0.04
11	42067	USM3M02	-88.649	30.043	0.62
12	AMRL1	LAWMA, Amerada Pass, LA	-91.338	29.45	0.08
13	BABT2	Baffin Bay, TX	-97.405	27.297	-0.57
14	BKTL1	Lake Charles Bulk Terminal, LA	-93.296	30.194	0.07
15	CAPL1	Calcasieu, La	-93.343	29.768	0.52
16	CARL1	Carrollton, LA	-90.135	29.933	0.52
17	EINL1	North of Eugene Island, LA	-91.384	29.373	0.12
18	EPTT2	Eagle Point, TX	-94.917	29.481	-0.77
19	FCGT2	USCG Freeport, TX	-95.303	28.943	-0.04
20	FRWL1	Fresh Water Canal Locks, La	-92.305	29.555	-0.11
21	GISL1	Grand Isle, LA	-89.958	29.265	-0.42
22	GNJT2	Galveston Bay Entrance (North Jetty), TX	-94.725	29.357	0.22
23	IRDT2	South Bird Island, TX	-97.322	27.48	-0.58
24	LCLL1	Lake Charles, La	-93.222	30.223	0.41
25	MBET2	Matagorda Bay Entrance Channel, TX	-96.327	28.422	0.39
26	MCGA1	Coast Guard Sector Mobile, AL	-88.058	30.649	0.17
27	MGPT2	Morgans Point, TX	-94.985	29.682	-0.09
28	MQTT2	Bob Hall Pier, Corpus Christi, Tx	-97.217	27.58	-0.08
29	NUET2	Nueces Bay, TX	-97.486	27.832	-0.37
30	NWCL1	New Canal Station, LA	-90.113	30.027	0.34
31	OBLA1	Mobile State Docks, AL	-88.04	30.705	0.11
32	PACT2	Packery Channel, TX	-97.237	27.634	-0.34
33	PCBF1	Panama City Beach, FL	-85.88	30.213	0.36
34	PCLF1	Pensacola, FL	-87.212	30.403	0.38
35	PILL1	Pilottown, LA	-89.259	29.179	0.38
36	PMNT2	Port Mansfield, TX	-97.424	26.559	-1.06
37	PNLM6	Pascagoula NOAA Lab, MS	-88.567	30.358	0.53
38	PORT2	Port Arthur, TX	-93.93	29.867	0.48
39	PTAT2	Port Aransas, TX	-97.05	27.828	-0.23
40	PTIT2	Port Isabelle, TX	-97.215	26.06	-0.01
41	RCPT2	Rockport, TX	-97.048	28.024	0.17
42	RLIT2	Realitos Peninsula, TX	-97.285	26.262	-0.21
43	RSJT2	Rincon del San Jose, TX	-97.471	26.801	0.51
44	RTAT2	Port Aransas, TX	-97.073	27.84	0.77
45	SBPT2	Sabine Pass North, TX	-93.87	29.73	-0.08
46	SDRT2	Seadrift, TX	-96.712	28.407	-0.27
47	SHBL1	Shell Beach, LA	-89.673	29.868	-0.04
48	TESL1	Tesoro Marine Terminal, Berwick, Atchafalaya River, LA	-91.237	29.668	0.62
49	TXPT2	Texas Point, Sabine Pass, TX	-93.842	29.689	0.08
50	ULAM6	Dock East Port of Pascagoula, MS	-88.505	30.348	-0.57
51	VCAT2	Port Lavaca, TX	-96.595	28.64	0.07
52	WBYA1	Weeks Bay, Mobile Bay, AL	-87.825	30.417	0.52

References

1. Etter, P.C.; Ulm, W.F.; Cochrane, J.D. The relationship of the wind stress to heat flux divergence of Texas-Louisiana shelf waters. *Cont. Shelf Res.* **1986**, *4*, 547–552. [[CrossRef](#)]
2. Morey, S.; Zavala-Hidalgo, J.; O'Brien, J.J. The seasonal variability of continental shelf circulation in the Northern and Western Gulf of Mexico from a high-resolution numerical model. In *Circulation in the Gulf of Mexico: Observations and Models*; Sturges, M., Lugo-Fernandez, A., Eds.; American Geophysical Union: Washington, DC, USA, 2005; pp. 203–218.
3. Sturges, W.; Lugo-Fernandez, A. *Circulation in the Gulf of Mexico: Observations and Models*; American Geophysical Union: Washington, DC, USA, 2005.

4. Westerink, J.J.; Muccino, J.C.; Luettich, R.A. Resolution requirements for a tidal model of the Western North Atlantic and Gulf of Mexico. In *Computational Methods in Water Resources IX, Volume 2: Mathematical Modeling in Water Resources*; Russell, T.F., Ewing, R.E., Brebbia, C.A., Gray, W.G., Pinder, G.F., Eds.; Computational Mechanics Publications: Southampton, UK, 1992; pp. 669–674.
5. Longley, W.L. *Freshwater inflows to Texas Bays and Estuaries, Ecological Relationships and Methods for Determination of Needs*; Texas Water Development Board and Texas Parks and Wildlife Department: Austin, TX, USA, 1994; p. 386.
6. Hofmann, E.E.; Worley, S.J. An investigation of the circulation of the Gulf of Mexico. *J. Geophys. Res.* **1986**, *91*, 14221–14236. [[CrossRef](#)]
7. Dinnel, S.P.; Wiseman, W.J. Freshwater on the west Louisiana and Texas shelf. *Cont. Shelf Res.* **1986**, *6*, 765–784. [[CrossRef](#)]
8. Dzwonkowski, B.; Park, K. Subtidal circulation on the Alabama shelf during the Deepwater Horizon oil spill. *J. Geophys. Res.* **2012**, *117*, C03027. [[CrossRef](#)]
9. Elliott, B.A. Anticyclonic rings in the Gulf of Mexico. *J. Phys. Oceanogr.* **1982**, *12*, 1292–1309. [[CrossRef](#)]
10. Kelly, F.J. Physical oceanography/water mass characterization. In *Mississippi-Alabama Continental Shelf Ecosystem Study: Data Summary and Synthesis. Volume II: Technical Narrative*; Brooks, J.M., Giammona, C.P., Eds.; U.S. Dept. of the Interior, Minerals Mgmt. Service, Gulf of Mexico OCS Region: New Orleans, LA, USA, 1991.
11. Zhang, Z.; Hetland, R.D. A numerical study on convergence of alongshore flows over the Texas-Louisiana shelf. *J. Geophys. Res.* **2012**, *117*, C11010. [[CrossRef](#)]
12. Zhang, X.; Marta-Almeida, M.; Hetland, R.D. A high-resolution pre-operational forecast model of circulation on the Texas-Louisiana continental shelf and slope. *J. Oper. Oceanogr.* **2012**, *5*, 1–16. [[CrossRef](#)]
13. Zhang, Z.; Hetland, R.; Zhang, X. Wind-modulated buoyancy circulation over the Texas-Louisiana shelf. *J. Geophys. Res. Oceans* **2014**, *119*, 5705–5723. [[CrossRef](#)]
14. Wiseman, W.J.; Rabalais, N.N.; Turner, R.E.; Dinnel, S.P.; MacNaughton, A. Seasonal and interannual variability within the Louisiana coastal current: Stratification and hypoxia. *J. Mar. Syst.* **1997**, *12*, 237–248. [[CrossRef](#)]
15. DiMarco, S.F.; Howard, M.K.; Reid, R.O. Seasonal variation of wind-driven diurnal current cycling on the Texas-Louisiana Continental Shelf. *Geophys. Res. Lett.* **2000**, *27*, 1017–1020. [[CrossRef](#)]
16. Burchard, H.; Hetland, R. Quantifying the Contributions of Tidal Straining and Gravitational Circulation to Residual Circulation in Periodically Stratified Tidal Estuaries. *J. Phys. Oceanogr.* **2010**, *40*, 1243–1262. [[CrossRef](#)]
17. Chen, C.; Liu, H.; Beardsley, R. An unstructured grid, finite-volume, three dimensional primitive equations ocean model: Application to coastal ocean and estuaries. *J. Atmos. Oceanic Technol.* **2003**, *20*, 159–186. [[CrossRef](#)]
18. Wei, E.; Yang, Z.; Chen, Y.; Kelley, J.W.; Zhang, A. *The Northern Gulf of Mexico Operational Forecast System (NGOFS): Model Development and Skill Assessment*; NOAA Technical Report NOS CS33; NOAA: Silver Spring, MD, USA, 2014.
19. Wei, E.; Zhang, A.; Yang, Z.; Chen, Y.; Kelley, G.W.; Aikman, F.; Cao, D. NOAA's Nested Northern Gulf of Mexico operational forecast systems development. *J. Mar. Sci. Eng.* **2014**, *2*, 1–17. [[CrossRef](#)]
20. Zhang, A.; Yang, Z. *High Performance Computer Coastal Ocean Modeling Framework for the NOS Coastal Operational Forecast System*; NOAA Technical Report NOS CO-OPS 069; U.S. Department of Commerce: Silver Spring, MD, USA, 2014. Available online: https://tidesandcurrents.noaa.gov/publications/NOAA_Technical_Report_NOS_COOPS_069.pdf (accessed on 1 June 2018).
21. Zhang, A.; Hess, K.W.; Wei, E.; Myers, E. *Implementation of Model Skill Assessment Software for Water Level and Current*; NOAA Technical Report NOS CS 24; U.S. Department of Commerce, National Oceanic and Atmospheric Administration: Silver Spring, MD, USA, 2006.
22. Mellor, G.L.; Yamada, T. Development of a turbulence closure model for geophysical fluid problems. *Rev. Geophys.* **1982**, *20*, 851–875. [[CrossRef](#)]
23. Smagorinsky, J. General circulation experiments with the primitive equations I. the basic experiment. *Mon. Weather Rev.* **1963**, *91*, 99–164. [[CrossRef](#)]
24. Chen, C.; Gao, G.; Zhang, Y.; Beardsley, R.C.; Lai, Z.; Qi, J.; Lin, H. Circulation in the Arctic Ocean: Results from a high-resolution coupled ice-sea nested Global-FVCOM and Arctic-FVCOM system. *Prog. Oceanogr.* **2015**, *141*, 60–80. [[CrossRef](#)]

25. Zheng, L.; Weisberg, R.H. Modeling the West Florida coastal ocean by downscaling from the deep ocean, across the continental shelf and into the estuaries. *Ocean Modell.* **2012**, *48*, 10–29. [CrossRef]
26. Zhao, L.; Chen, C.; Cowles, G. Tidal flushing and eddy formation in Mount Hope Bay and Narragansett Bay: An application of FVCOM. *J. Geophys. Res.* **2006**, *111*, C10015. [CrossRef]
27. Zheng, L.Y.; Weisberg, R.H. Rookery Bay and Naples Bay circulation simulations: applications to tides and fresh water inflow regulation. *Ecol. Model.* **2010**, *221*, 986–996. [CrossRef]
28. Yang, Z.; Myers, E.; White, S. *VDatum for Eastern Louisiana and Mississippi Coastal Waters: Tidal Datums, Marine Grids, and Sea Surface Topography*; NOAA Technical Memorandum NOS CS 19; U.S. Department of Commerce: Silver Spring, MD, USA, 2010. Available online: https://vdatum.noaa.gov/download/publications/CS_19_FY09_26_Zizang_VDatum_NewOrleans_techMemor.pdf (accessed on 16 June 2018).
29. Szpilka, C.; Dresback, K.; Kolar, R.; Feyen, J.; Wang, J. Improvements for the Western North Atlantic, Caribbean and Gulf of Mexico ADCIRC tidal database (EC2015). *J. Mar. Sci. Eng.* **2016**, *4*, 72. [CrossRef]
30. Mehra, A.; Rivin, I.; Garraffo, Z.; Rajan, B. Upgrade of the Operational Global Real Time Ocean Forecast System. Available online: https://www.wcrp-climate.org/WGNE/BlueBook/2015/individual-articles/08_Mehra_Avichal_et_al_RTOFS_Upgrade.pdf (accessed on 29 October 2016).
31. Garaffo, Z.D.; Kim, H.C.; Mehra, A.; Spindler, T.; Rivin, I.; Tolman, H.L. Modeling of ¹³⁷Cs as a tracer in a regional model for the Western Pacific, after the Fukushima-Daiichi Nuclear power plant accident of March 2011. *Weather Forecast.* **2016**, *21*, 553–579. [CrossRef]
32. U.S. Geological Survey (USGS). USGS Water Data for the Nation. Available online: <http://waterdata.usgs.gov/nwis/> (accessed on 15 October 2013).
33. Cowles, G.W.; Lentz, S.J.; Chen, C.; Xu, Q.; Beardsley, R.C. Comparison of observed and model-computed low frequency circulation and hydrography on the New England Shelf. *J. Geophys. Res.* **2008**, *113*, C09015. [CrossRef]
34. Center for Operational Oceanographic Products and Services (CO-OP). Water Levels—Station Selection. Available online: <http://tidesandcurrents.noaa.gov/stations.html?type=Water+Levels> (accessed on 18 March 2018).
35. National Data Buoy Center (NDBC). Archive of Historical Ocean Data. Available online: <http://www.ndbc.noaa.gov/data/historical/ocean/> (accessed on 18 March 2018).
36. Taylor, K.E. Summarizing multiple aspects of model performance in a single diagram. *J. Geophys. Res.* **2001**, *106*, 7183–7192. [CrossRef]
37. National Center for Atmospheric Research Staff (Ed.) The Climate Data Guide: Taylor Diagrams. Available online: <https://climatedataguide.ucar.edu/climate-data-tools-and-analysis/taylor-diagrams> (accessed on 18 October 2018).
38. Dawson, C.W.; Wilby, R.L. Hydrological modelling using artificial neural networks. *Prog. Phys. Geogr.* **2001**, *25*, 80–108. [CrossRef]
39. Dawson, C.W.; Abraham, R.J.; See, L.M. HydroTest: A web-based toolbox of evaluation metrics for the standardized assessment of hydrological forecasts. *Environ. Mode. Softw.* **2007**, *22*, 1034–1052. [CrossRef]
40. Jain, A.; Srinivasulu, S. Development of effective and efficient rainfall-runoff models using integration of deterministic, real-coded genetic algorithms and artificial neural network techniques. *Water Resour. Res.* **2004**, *40*. [CrossRef]

